Pressure- and photoinduced transformation into a metastable phase in $RbMn[Fe(CN)_6]$

Y. Moritomo and M. Hanawa
Department of Applied Physics, Nagoya University, Nagoya 464-8603, Japan and PRESTO, JST

Y. Ohishi, K. Kato, and M. Takata
SPring-8/JASRI, Hyogo 679-5198, Japan

A. Kuriki
Department of Crystalline Materials Science, Nagoya University, Nagoya 464-8603, Japan

E. Nishibori and M. Sakata
Department of Applied Physics, Nagoya University, Nagoya 464-8603, Japan

S. Ohkoshi, H. Tokoro, and K. Hashimoto
Research Center for Advanced Science and Technology, University of Tokyo, Tokyo 153-8904, Japan
(Received 25 February 2003; revised manuscript received 14 May 2003; published 15 October 2003)

Pressure and photoirradiation effects on the structural properties were investigated for a transition metal cyanide, $RbMn[Fe(CN)_6]$, with perovskitelike structure by means of high-angle resolved synchrotron-radiation x-ray powder diffraction. We have found that (1) photoirradiation by a 532-nm pulse laser at 91 K and (2) application of hydrostatic pressure to about 2 GPa at 300 K change the system from the tetragonal low-temperature phase ($I\bar{4}m2$; $Z=2$) to a metastable state with different crystal symmetry ($P\bar{4}n2$; $Z=2$). We discuss the difference between the photoinduced and pressure-induced processes and suggest possible origin for the photoinduced demagnetization.

DOI: 10.1103/PhysRevB.68.144106 PACS number(s): 64.60.My, 61.50.Ks

I. INTRODUCTION

Transition-metal cyanides (the so-called Prussian-blue compounds), $A(\mathrm{I})M(\mathrm{II})[N(\mathrm{III})(CN)_6]$ ($A=$Na, K, Rb, Cs; $N=$Mn, Co, Cr; $M=$Fe, Cr),[1–9] have been attracting renewed interest of materials scientists, because they show a photoinduced magnetization/demagnetization. For example, Sato *et al.*[3] reported the enhancement of magnetization in $K_{0.2}Co_{1.4}Fe(CN)_6 6.9H_2O$ by irradiation of a red light (660 nm) at 5 K and suppression of magnetization by irradiation of a blue light (450 nm) at 5 K. This photoinduced magnetism has been ascribed to the photoinduced structural change into some *metastable state* and the resultant variation of the electronic configuration of the transition metals. Then, determination of the crystal structure, including atomic coordinates, is indispensable for a deeper comprehension of the photoinduced phenomena as well as their practical application.

The Prussian-blue compounds are well known from the earliest times. Nevertheless, except for $Fe_4[Fe(CN)_6]_3 15H_2O$,[10] difficulty in crystal growth has prevented detailed structural investigations of these compounds. In addition, the compounds contain considerable nonstoichiometric H_2O molecules, which makes the precise structural analysis difficult. Recently, Ohkoshi *et al.*[11] synthesized a Mn-Fe compound, $RbMn[Fe(CN)_6]$, which does not contain extra H_2O molecules. Neutron powder-diffraction experiment[12] revealed that $RbMn[Fe(CN)_6]$ is ferromagnetic below $T_C=12$ K, where the local spin moments are taken only by the high-spin (HS) Mn^{2+} ($S=2$) ions. Furthermore, Tokoro *et al.*[13] observed suppression of magnetization by irradiation of a visible pulse laser (532 nm) at 3 K. Therefore, $RbMn[Fe(CN)_6]$ is one of the most suitable compounds for detailed structural investigation to reveal the origin for the photoinduced demagnetization.

At room temperature, $RbMn[Fe(CN)_6]$ is face-centered cubic ($F\bar{4}3m$: $Z=4$).[11,14] Reflecting the stability of the HS Mn^{2+} state, the valence state is HS Mn^{2+} (d^5; $S=5/2$)–low-spin (LS) Fe^{3+} (d^5; $S=1/2$).[11] With decrease of temperature below 220 K, however, a structural transition from the cubic phase to the body-centered tetragonal ($I\bar{4}m2$; $Z=2$) phase takes place, accompanying the Jahn-Teller type distortion of the MnN_6 octahedra. Therefore, the cubic-to-tetragonal structural transition is considered to be driven by *charge transfer*[14] from the Mn^{2+} site to the Fe^{3+} site. Consistently, Osawa *et al.*[15] proposed that the low-temperature valence state is HS Mn^{3+} (d^4; $S=2$)–LS Fe^{2+} (d^6; $S=0$), based on their x-ray emission and absorption spectra. Hereafter, we denote the high-temperature cubic phase ($F\bar{4}3m$; $Z=4$) and the low-temperature tetragonal phase ($I\bar{4}m2$; $Z=2$) as HT and LT phases, respectively.

In this paper, we report the crystal structure of a thermally quenched metastable state of $RbMn[Fe(CN)_6]$ determined by synchrotron-radiation x-ray powder diffraction (XRD). The metastable state belongs to the tetragonal space group ($P\bar{4}n2$; $Z=2$), which is different from those of the HT phase and the LT phase. In the metastable phase, the ligand CN^- ions approach the Mn site accompanied by the tilting of the in-plane ions along the c direction. We further found that

(1) photoirradiation by a 532-nm pulse laser at 91 K and (2) application of hydrostatic pressure about 2 GPa at 300 K change the system into the metastable state.

II. EXPERIMENT

A. Sample preparation

$RbMn[Fe(CN)_6]$ was prepared by reacting an aqueous solution ($0.1\ \mathrm{mol\,dm^{-3}}$) of $MnCl_2$ with a mixed aqueous solution of $RbCl_3$ ($1\ \mathrm{mol\,dm^{-3}}$) and $K_3[Fe(CN)_6]$ ($0.1\ \mathrm{mol\,dm^{-3}}$) to yield a light-brown precipitate.[11] Elemental analysis by inductively coupled plasma-atomic emission spectroscopy revealed that the atomic mol ratio is nearly the ideal value: Rb:Mn:Fe=0.98:1.01:1.

B. Synchrotron-radiation x-ray powder diffraction

To obtain x-ray powder data of good statistics with high angular resolution, XRD measurements were carried out at SPring-8, BL02B2 beamline (temperature dependence and photoirradiation effects)[16] and BL10XU (pressure dependence) beamline. The as-grown sample powders were fine enough, and gave a homogeneous intensity distribution in the Debye-Scherrer powder ring. The homogeneity of the ring is a necessary condition for a reliable Rietveld analysis.

At the BL02B2 beamline, the sample powders were sealed in a quartz capillary whose temperature was controlled using nitrogen gas in the range from 91 K to 340 K. The reflections were collected on an imaging plate installed on a large Debye-Scherrer camera ($r=286.5$ mm). The wavelength of the incident x ray was about 0.82 Å (near below the *K* edge of Rb), and typical exposure time was 30 min. Actual wavelength was calibrated with use of a standard CeO_2 powder obtained from NIST. In the measurements of the ''photoirradiated'' pattern, glass powders were mixed so that the 532-nm pulse laser homogeneously excites the respective sample powders. Note that the penetration depth at this photon energy is much shallower (about 1 μm).

High-pressure XRD was performed at BL10XU beamline at room temperature using a specially designed diamond anvil cell (DAC).[17] The sample powders were sealed in a gasket hole of the DAC, about 100 μm in thickness and about 200 μm in diameter, which was filled with Fluorinert (made by Sumitomo 3M) as a pressure-transmitting medium. The 2θ range used in the Rietveld analysis is $4°-25°$. In order to get Debye-Scherrer powder rings with homogeneous intensity distribution, the DAC was rotated $\pm 5°$ along the ω axis. Magnitude of the applied pressure was monitored by the wavelength of the luminescence line R_1 (Ref. 18) from a small piece of ruby placed in the gasket hole. The wavelength of the incident x ray was 0.4951 Å, and the exposure time was 10 min.

C. Rietveld analysis

The powder patterns obtained were analyzed by a Rietveld structure refinement program [RIETAN2000 (Ref. 19)]. We show in Fig. 1(a) an example of the Rietveld refinement of XRD pattern of $RbMn[Fe(CN)_6]$ at 300 K. The powder pattern was analyzed with the cubic model ($F\bar{4}3m$; $Z=4$), in which the Rb can locate either at $4c$ or at $4d$ sites. The occupancy g [$=0.908(2)$] at the $4c$ site was determined by the Rietveld refinement, and is fixed in the analysis presented in this paper. Based on the elemental analysis, g of the Mn site was fixed at 1.01. We assume that C (N) atoms surround Fe (Mn) atom.

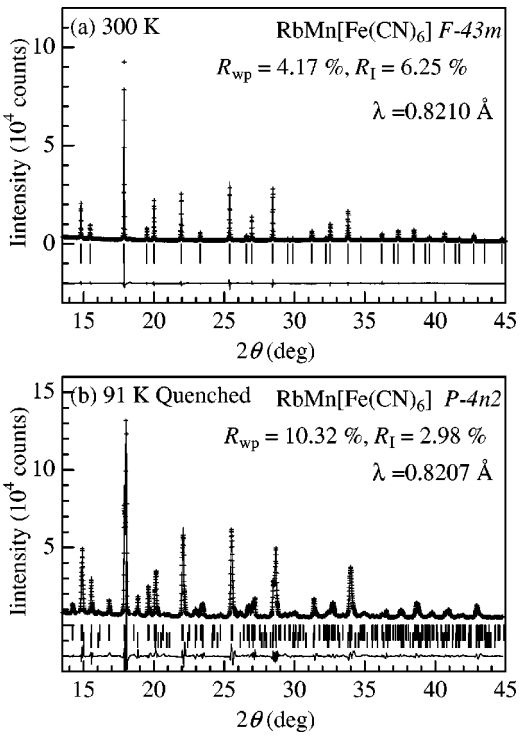

FIG. 1. X-ray-diffraction patterns of $RbMn[Fe(CN)_6]$: (a) at 300 K, and (b) of thermally quenched sample at 91 K. Solid curves represent the results of the Rietveld refinement with (a) cubic ($F\bar{4}3m$; $Z=4$) and (b) two-phase model with $P\bar{4}n2$ (90%) and $I\bar{4}m2$ (10%).

III. RESULTS

A. Structure of the metastable phase

Figure 1(b) shows the powder pattern of the metastable state of $RbMn[Fe(CN)_6]$ at 91 K, which was obtained by rapid cooling of the powder sample in a quartz capillary by cold N_2 gas. The overall appearance of the powder pattern is similar to that of the HT phase at 300 K [Fig. 1(a)]. Consistently, Tokoro *et al.*[20] investigated infrared absorption spectra of the thermally quenched sample, and found that the spectra are almost the same as that of the HT phase. We, however, observed splittings and shoulder structures in several Bragg reflections in the large-2θ region, which can be well reproduced by a tetragonal cell ($\sqrt{2}a \approx c \approx a_{300\ \mathrm{K}}$). In addition, we observed rather intense 210 and 212 reflections in the tetragonal setting, which are forbidden in $I\bar{4}m2$ symmetry. We have investigated the subgroup of $I\bar{4}m2$, i.e., $I\bar{4}$, $Imm2$, $F222$, $P\bar{4}m2$, and $P\bar{4}n2$. (The 210 and 212 reflections are forbidden also in $I\bar{4}$, $Imm2$, and $F222$.) We finally

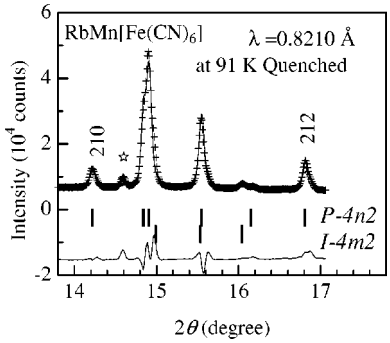

FIG. 2. Magnified portion of the XRD patterns of the thermally quenched $RbMn[Fe(CN)_6]$ at 91 K. Solid curves represent Rietveld fit with a $P\bar{4}n2$ and $I\bar{4}m2$ two-phase model, and crosses represent experimental data. The star indicates diffraction from ice crystals formed out of the capillary.

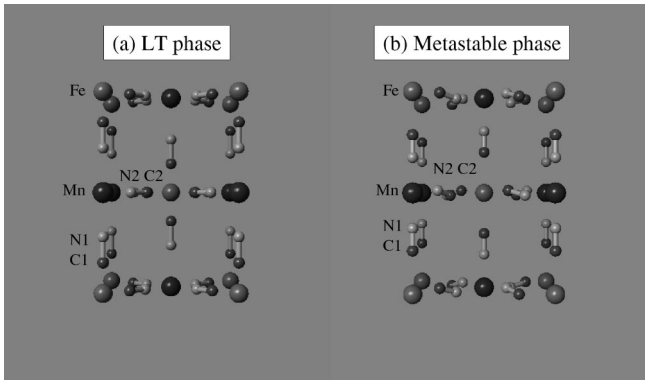

FIG. 3. Crystal structure: (a) low-temperature (LT) phase ($I\bar{4}m2$: $Z=2$) and (b) metastable phase ($P\bar{4}n2$: $Z=2$). Rb^+ ions are omitted.

found that the $P\bar{4}n2$ model satisfactorily reproduces the intensity of the extra reflections (see the magnified segment of the powder pattern in Fig. 2). In the Rietveld analysis, we adopted a two-phase model with $P\bar{4}n2$ and $I\bar{4}m2$ (LT phase), as shown in Fig. 1(b). The mass fraction s of the metastable phase ($P\bar{4}n2$) is 0.90. We list in Table I the atomic coordinates the of metastable phase.[22] The reliability factors R_{wp} and R_I for the metastable phase are 10.32% and 2.98%, respectively.

In order to clarify the structural difference between the LT phase and the metastable phase, we show in Fig. 3 ball-and-stick models based on the experimentally determined atomic coordinates. In the metastable phase, the ligand CN^- ions approach the Mn site accompanied by the tilting of the in-plane CN^- ions (C2-N2) along the c direction. In Table II, we compare the in the Mn-N and Fe-C bond distances in the metastable structure with those in the LT phase. In the metastable phase (1) the average Mn-N distance [$=1.901(17)$ Å] is shorter, while $\bar{d}_{Fe\text{-}C}$ ($=2.250(23)$ Å) is longer, than that in the LT phase, and (2) the Jahn-Teller type distortion of the MnN_6 octahedra in the LT phase nearly disappears. These structural features, as well as the infrared absorption spectra,[20] of the metastable phase suggest that the valence state is Mn^{2+} (d^5)–Fe^{3+} (d^5).

TABLE I. Atomic coordinates, equivalent displacement parameters U, and occupancy g for the metastable phase of $RbMn[Fe(CN)_6]$ at 91 K. The space group is $P\bar{4}n2$ ($Z=2$). Lattice constants are $a=7.410\,70(30)$ Å and $c=10.548\,11(47)$ Å. U for Mn is fixed at the value of Fe, while those for C2, N1, N2 are fixed at the value of C1. U for Rb2 is fixed at the value of Rb1. $R_{wp}\{\equiv[\Sigma_i w_i(y_i-y_{i,calc})^2/\Sigma_i w_i y_i^2]^{1/2}\}$ and $R_I(\equiv\Sigma_K|I_{K,calc}-I_K|/\Sigma_K I_{K,calc})$ are 10.32% and 2.98%, respectively.

Atom	site	g	x	y	z	U(Å^2)
Fe	2a	1.01	0	0	0	0.0097(5)
Mn	2b	1	0	0	1/2	0.0097
Rb1	2c	0.908	0	1/2	1/4	0.0579(5)
Rb2	2d	0.072	0	1/2	3/4	0.0579
C1	4e	1	0	0	0.220(2)	0.0063(10)
C2	8i	1	0.178(3)	0.248(3)	0.014(2)	0.0063
N1	4e	1	0	0	0.328(2)	0.0063
N2	8i	1	0.296(2)	0.337(3)	−0.016(2)	0.0063

B. Pressure-induced transformation into the metastable phase

We show in Fig. 4 pressure variation of the XRD patterns of $RbMn[Fe(CN)_6]$ at 300 K in the pressure-increasing run. (The 2θ range nearly corresponds to Fig. 2.) Here, let us tentatively classify the powder patterns into three pressure (P) regions, for the convenience of explanation: $P \leqslant 0.3$ GPa (region I), 0.3 GPa$\leqslant P \leqslant$1.9 GPa (region II), and 1.9 GPa$\leqslant P$ (region III).

At $P=0.16$ GPa (thick curve in Fig. 4, region I), most of the reflections can be indexed in the face-centered cubic cell (HT phase). We, however, observed several weak reflections (e.g., at 9.0° and 9.6°), which can be indexed in the body-centered tetragonal setting (LT phase). So, we analyzed the powder pattern with HT-LT two-phase model. The mass fraction of the HT phase is 0.68. The reliability factors R_{wp} and R_I for the HT phase are 5.20% and 7.72%, respectively. Here, we note that the HT-to-LT structural transition of $RbMn[Fe(CN)_6]$ shows large thermal hysteresis (220 K–300 K).[14] So, the system at 300 K and at 0.16 GPa can be present in the bistable region, and tends to become two-phase state.

TABLE II. The Mn-N and Fe-C bond distances for the metastable (M:$P\bar{4}n2$; $Z=2$) and low-temperature (LT: $I\bar{4}m2$; $Z=2$) phases.

Phase	M at 91 K Å	LT at 100 K Å
Mn-N1	1.818(19)	2.283(17)
Mn-N2	1.943(16)	1.907(32)
Mn-N (average)	1.901(17)	2.032(27)
Fe-C1	2.298(24)	1.855(22)
Fe-C2	2.226(22)	1.979(40)
Fe-C (average)	2.250(23)	1.938(34)

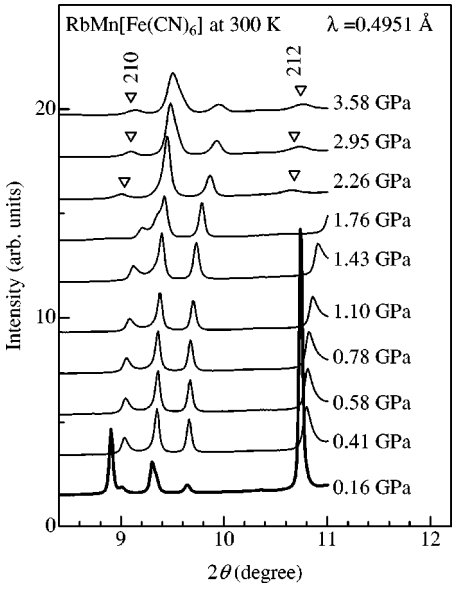

FIG. 4. Pressure variation of the XRD patterns (crosses) at 300 K in the pressure-increasing run. Open triangles indicate 210 and 212 reflections, which are forbidden in $I\bar{4}m2$ symmetry.

The powder patterns in region II are analogous to that of the LT phase. We, however, failed to reproduce the powder pattern by Rietveld refinement with LT single-phase model; in particular, we can not reproduce the intensity of the 202 reflection observed at 9.6°.[23] Here, note that the 210 and 212 reflections (indicated by open triangles) observed in region III are due to $P\bar{4}n2$ phase (metastable phase). So, we adopted an LT-metastable phase two-phase model for the analysis of the powder patterns both in region II and region III. We list in Table III mass fractions *s* of the LT phase and the metastable phase against *P* together with reliability parameters R_{wp} and R_I. *s* of the metastable phase is nearly constant (0.2–0.3) below $P=1.10$ GPa. With further increase of *P* beyond 1.43 GPa, *s* steeply increases and reaches about 0.8 at $P=2.26$ GPa. Thus, the crossover pressure for the LT-to-metastable structural transition is at 1.4–1.8 GPa at 300 K.

TABLE III. Pressure variation of mass fractions *s* of the LT phase and the metastable phase determined by LT-metastable two-phase Rietveld analysis. R_{wp} and R_I for the respective phases are also listed. The $P=0.33$-GPa data were obtained after the pressure-increasing run.

Pressure (GPa)	R_{wp}	LT		*M*	
		s	R_I	*s*	R_I
0.41	4.29	0.77	5.20	0.23	5.56
0.58	4.55	0.75	4.86	0.25	5.05
0.78	4.44	0.74	4.78	0.26	4.93
1.10	4.42	0.70	5.03	0.30	5.05
1.43	4.14	0.59	5.29	0.41	6.06
1.76	4.54	0.44	5.76	0.56	5.98
2.26	4.03	0.19	4.76	0.81	5.54
2.95	3.72	0.08	3.74	0.92	4.12
3.58	3.15			1	2.36
0.33	4.11	0.72	5.89	0.28	5.93

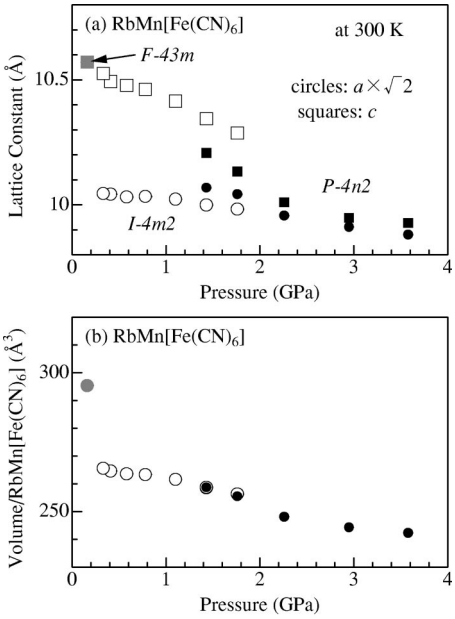

FIG. 5. (a) Lattice constants and (b) volume per chemical formula at 300 K against pressure. Gray, open, and filed symbols represent the high-temperature ($F\bar{4}3m$; $Z=4$), low-temperature ($I\bar{4}m2$; $Z=2$), and metastable ($P\bar{4}n2$; $Z=2$) phases, respectively. The $P=0.33$-GPa data were obtained after the pressure-increasing run.

In Fig. 5 we thus obtained (a) lattice constants and (b) volume per chemical formula for $RbMn[Fe(CN)_6]$ at 300 K against *P*. With increase of *P*, HT-to-LT phase transition takes place at about 0.3 GPa in the *P*-increasing run. As shown in the lower panel, the HT-to-LT phase transition accompanies about 10% reduction of volume. In the tetragonal phase ($P \geqslant 0.4$ GPa), the lattice constants gradually decrease in an anisotropic manner: initial pressure coefficient ($P \leqslant 1$ GPa) of *a* ($\equiv -1/a\,da/dP = 1.0\%/\mathrm{GPa}$) is three times larger than that of *c* ($=0.3\%/\mathrm{GPa}$). Reduction of *a* becomes steeper when *P* exceeds about 1.4–GPa, and eventually a pseudocubic structure ($a\sqrt{2} \approx c$; metastable phase) appears at about 2 GPa.

We further investigated the pressure dependence of T_C up to ≈ 1 GPa with use of a piston-cylinder type clamp cell. The sample powders were sealed in the cylinder, about 3 mm in length and 2.0 mm in diameter, which was filled with Fluorinert (made by Sumitomo 3M) as a pressure-transmitting medium. The applied pressure *P* was calibrated by the superconducting transition temperature of Pb ingot placed in the sample room. We found that T_C increases linearly with *P* as $T_C = 11.8 + 1.3P(\mathrm{GPa})$. The enhanced T_C is ascribed to the shortened bond distances between the Mn site and the Fe site, which enhance the exchange interactions.

C. Photoinduced transformation into the metastable phase

In addition to pressure, a photoirradiation by a 532-nm pulse laser also transforms the LT phase to the metastable

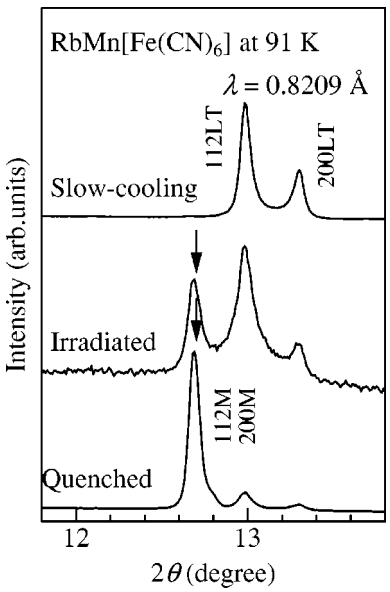

FIG. 6. X-ray diffraction patterns at 91 K. Arrows indicate the Bragg reflection due to the metastable phase. The ''quenched'' patterns was obtained after rapid cooling of sample in a quartz capillary by cold N_2 gas, and ''irradiated'' patterns was obtained after irradiation by a visible pulse laser (10 Hz, 10 mJ, 532 nm) for 10 min at 91 K.

phase. Figure 6 shows the x-ray powder patterns of $RbMn[Fe(CN)_6]$ at 91 K after various thermal- and photohystereses. ''Quenched'' pattern (bottom) is obtained by rapid cooling of the powders by cold N_2 gas: the intense reflection indicated by a downward arrow is due to the 112 and 200 reflections of the tetragonal metastable phase. ''Irradiated'' pattern (middle) is obtained by irradiation of sample powders by a visible pulse laser (10 Hz, 10 mJ, 532 nm) for 10 min at 91 K. One may observe a new reflection (downward arrow), suggesting a photoinduced structural transformation. Actually, the irradiated powder pattern ($12° \leqslant 2\theta \leqslant 45°$) is well reproduced by the Rietveld fitting with the two tetragonal phases.

We show in Fig. 7 temperature dependence of lattice constants a (circles) and c (squares), and mass fraction (filled triangles) of the two tetragonal phases after (a) thermal-quenching and (b) photoirradiation. Lattice constants of the

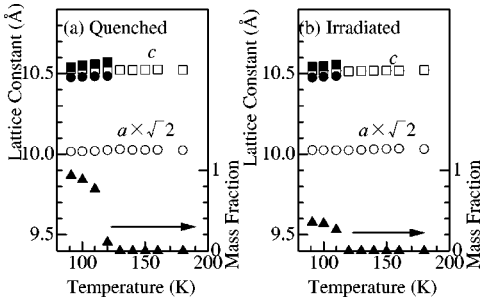

FIG. 7. Temperature dependence of lattice constants, a (circles) and c (squares), and mass fraction (filled triangles) of the metastable phase after (a) thermal quenching and (b) photoirradiation. Open symbols represent the lattice constants of the LT phase.

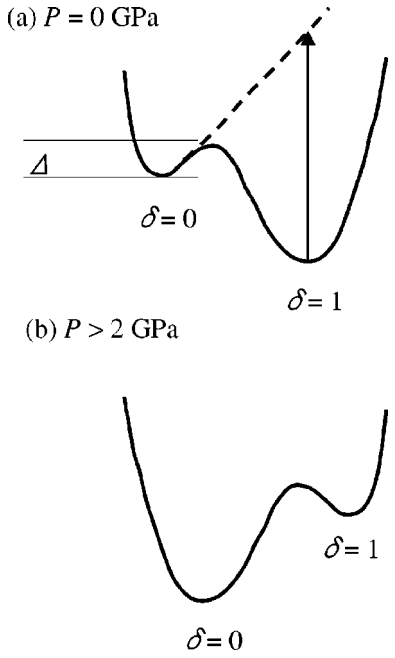

FIG. 8. Schematic picture for the free energy of the system at (a) $P=0$ GPa and (b) $P \geqslant 2$ GPa. δ means magnitude of the charge transfer from the Mn^{2+} site to the Fe^{3+} site. Δ is the potential barrier between the $\delta=0$ (metastable state) and $\delta=1$ (LT state) states. An upward arrow in (a) represents the photoinduced process via the Franck-Condon state.

phototransformed metastable phase [Fig. 7(a)] coincide with those of the thermally quenched one [Fig. 7(b)] within experimental error, suggesting that both the crystal structures are the same. Consistent with the above argument, both the metastable phases transform to the LT ground state at 120 K via the thermal activation process (see the mass fraction indicated by filled triangles).

IV. DISCUSSION

A. Comparison of the photoinduced process with the pressure-induced process

We schematically depict in Fig. 8(a) the free energy curve at ambient pressure ($P=0$ GPa), where the horizontal axis is the ligand coordinate. δ is the charge transfer from the Mn^{2+} site to the Fe^{3+} site: the $\delta=0$ ($\delta=1$) state corresponds to the metastable (LT) phase. We expect a local minimum at $\delta=0$, since the state is stabilized by the movement of the ligand CN^- ions toward the Mn site. Magnitude of the potential barrier Δ is of the order of 100 K, since the metastable phase relaxes to the ground state (LT phase) at 120 K (see Fig. 7).

The photoinduced process of the structural transition is as follows. The first process after the photoexcitation on the LT phase ($\delta=1$) is the charge transfer from the Fe^{2+} site to the Mn^{3+} site without ligand displacement [Franck-Condon state: see upward arrow in Fig. 8(a)]. Subsequently, the charge transfer triggers the ligand displacement toward the other local minimum at $\delta=0$ [broken curve of Fig. 8(a)]. The $\delta=0$ state would become more stable under strong ex-

citation, since the charge-transferred Fe^{3+}-Mn^{2+} pairs form a cluster. This cluster may be analogous to the critical nucleus,[24] which governs the crystallization process. Once the clusters are created, the subsequent photoexcitation would selectively excite the Fe^{2+}-Mn^{3+} pairs around the cluster surface. Thus, the photoinduced structural transformation takes place. Here, we note that a similar photoinduced process was reported also in the Na-Co-Fe-CN system.[21]

The above-mentioned photoinduced process is qualitatively different from the pressure-induced process, in which the free-energy curve itself is deformed to stabilize the $\delta=0$ state [see Fig. 8(b)]. As a result, the system continuously changes from the $\delta=1$ state to the $\delta=0$ state, as pressure increases. Looking at Fig. 5(b), one may notice that the cell volume ($=245$ Å^3) at 2.95 GPa is smaller than that (≈ 250 Å^3: extrapolation of the cell volume of the LT phase to 2.95 GPa) of the virtual LT phase ($\delta=1$). This indicates that the $\delta=0$ state becomes more stable than the $\delta=1$ state under pressure.

B. Magnetism of the metastable structure

We have tried to get information on magnetic properties of $RbMn[Fe(CN)_6]$ in the metastable phase. First, we tired to determine the magnetic properties of the metastable phase by a superconducting quantum interference device magnetometer with rapid quenching down to 4 K. The obtained state, however, contains considerable amount of the ferromagnetic LT phase, which prevents us from investigating the magnetic properties of the matestable phase. We further tried, but failed, to determine the magnetic structure of $RbMn[Fe(CN)_6]$ in the metastable phase by means of the neutron-diffraction experiments. Quite recently, Tokoro *et al.*[20] have found that Rb vacancy significantly stabilizes the thermally quenched metastable structure, and have investigated temperature variation of the magnetic susceptibility of $Rb_{0.7}Mn_{1.15}[Fe(CN)_6]2H_2O$ in the metastable phase. They found a kinklike structure at 13 K ($=T_N$), which suggests a antiferromagnetic spin ordering at T_N. We believe that $RbMn[Fe(CN)_6]$ in the metastable phase also shows the antiferromagnetic spin ordering.

Here, let us argue the possible spin structure of the metastable phase. Since the valence state of the metastable state is Fe^{3+} (d^5)–Mn^{2+} (d^5), the possible local spin moments are $S=5/2$, $S=3/2$, and $S=1/2$. Then, one may expect a simple NaCl-type antiferromagnetic spin structure mediated by superexchange interaction between Fe^{3+} and Mn^{2+} if the spin moments of Fe^{3+} and Mn^{2+} are the same. In this system, however, the Fe ions tend to take a lower spin configuration: actually, the valence state is HS Mn^{3+} (d^4; $S=2$)–LS Fe^{2+} (d^6; $S=0$) [HS Mn^{2+} (d^5; $S=5/2$)–LS Fe^{3+} (d^5; $S=1/2$)] in the HT (LT) phase.

Alternative spin structure may be an anisotropic one, reflecting the tetragonal symmetry of the metastable structure (see Fig. 3). Anisotropic structure is observed in several perovskite-type doped manganites $R_{1-x}A_xMnO_3$ (R and A are rare-earth and alkaline-earth metals, respectively) with a pseudocubic lattice structure. For example, a sheet-type antiferromagnetic spin structure is observed in $Nd_{0.45}Sr_{0.55}MnO_3$,[25] whereas a rod-type antiferromagnetic spin structure is observed in $Nd_{0.35}Sr_{0.65}MnO_3$.[25] These anisotropic spin structures have been ascribed to the subtle competition between the (antiferromagentic) superexchange and (ferromagnetic) double-exchange[26] interactions. Especially, in doped manganites, the ordering of the Mn $3de_g$ orbital causes the anisotropic transfer integral of the e_g electrons, which mediate the double-exchange interaction between the local t_{2g} spins: $d_{x^2-y^2}$ ($d_{3z^2-r^2}$) orbital-ordering caused the sheet-type (rod-type) antiferromagnetic spin structure. A similar scenario is applicable to the present system, because there exists t_{2g}-orbital degree of freedom in the LS Fe^{3+} (d^5).

V. SUMMARY

In summary, we have determined the metastable structure of $RbMn[Fe(CN)_6]$, which can be created by thermal quenching, photoirradiation, and application of pressure, by means of high-angle resolved XRD at SPring-8. The metastable state belongs to the tetragonal space group ($P\bar{4}n2$; $Z=2$), which is different from those of the high-temperature phase ($F\bar{4}3m$: $Z=4$) and the low-temperature phase ($I\bar{4}m2$; $Z=2$). We argued on the difference between the photoinduced and pressure-induced processes, and possible origin for the photoinduced demagnetization.

ACKNOWLEDGMENTS

This work was supported by a Grant-in-Aid for Scientific Research from the Ministry of Education, Culture, Sports, Science and Technology, Japan and from Asahi Glass Foundation. The synchrotron-radiation x-ray powder experiments were performed at the SPring-8 BL02B2 and BL10XU with the approval of the Japan Synchrotron Radiation Research Institute (JASRI).

[1] T. Mallah, S. Thiebaut, M. Verdaguer, and P. Veillet, Science **262**, 1554 (1993).

[2] O. Sato, T. Iyoda, A. Fujishima, and K. Hashimoto, Science **271**, 49 (1996).

[3] O. Sato, T. Iyoda, A. Fujishima, and K. Hashimoto, Science **272**, 704 (1996).

[4] O. Sato, Y. Einaga, T. Iyoda, A. Fujishima, and K. Hashimoto, J. Electrochem. Soc. **144**, L11 (1997).

[5] S. Ohkoshi and K. Hashimoto, J. Photochem. Photobio. **C2**, 71 (2001).

[6] S. Ferlay, T. Mallah, R. Ouahes, P. Veillet, and M. Verdaguer, Nature (London) **378**, 701 (1995).

[7] S. Ohkoshi, M. Mizuno, G.J. Hung, and K. Hashimoto, J. Phys. Chem. B **104**, 9365 (2000).

[8] S.M. Holmes and G.S. Girolami, J. Am. Chem. Soc. **121**, 5593 (1999).
[9] O. Hatlevik, W.E. Bushmann, J. Zhang, J.L. Manson, and J.S. Miller, Adv. Mater. **11**, 914 (1999).
[10] H.J. Buser, D. Schwarzenback, W. Petter, and A. Ludi, Inorg. Chem. **16**, 16 (1997).
[11] S. Ohkoshi, H. Tokoro, M. Utsunomiya, M. Mizuno, M. Abe, and K. Hashimoto, J. Phys. Chem. B **106**, 2423 (2002).
[12] Y. Moritomo, K. Kuriki, K. Ohoyama, H. Tokoro, S. Ohkoshi, K. Hashimoto, and N. Hamada, J. Phys. Soc. Jpn. **72**, 456 (2003).
[13] H. Tokoro, S. Ohkoshi, and K. Hashimoto, Appl. Phys. Lett. **82**, 1245 (2003).
[14] Y. Moritomo, K. Kato, A. Kuriki, M. Takata, M. Sakata, H. Tokoro, S. Ohkoshi, and K. Hashimoto, J. Phys. Soc. Jpn. **71**, 2078 (2002).
[15] H. Osawa, T. Iwazumi, H. Tokoro, S. Ohkoshi, K. Hashimoto, H. Shoji, E. Hirai, T. Nakamura, S. Nanao, and Y. Isozumi, Solid State Commun. **125**, 237 (2003).
[16] E. Nishibori, M. Takata, K. Kato, M. Sakata, Y. Kubota, S. Aoyagi, Y. Kuroiwa, M. Yamakawa, and N. Ikeda, Nucl. Instrum. Methods Phys. Res. A **467-468**, 1045 (2001).
[17] A. Kuriki, Y. Moritomo, A. Machida, E. Nishibori, M. Takata, M. Sakata, Y. Ohishi, O. Shimomura, and A. Nakamura, Phys. Rev. B **65**, 113105 (2002).
[18] H.K. Mao and P.M. Bell, Science **200**, 1145 (1978).
[19] F. Izumi and T. Ikeda, Mater. Sci. Forum **321-324**, 198 (2000).
[20] H. Tokoro, S. Ohkoshi, and K. Hashimoto (unpublished).
[21] M. Hanawa, Y. Moritomo, A. Kuriki, J. Tateishi, K. Kato, M. Takata, and M. Sakata, J. Phys. Soc. Jpn. **72**, 987 (2003).
[22] We obtained another structural solution by the Rietveld refinement with the $P\bar{4}n2$ model. In this structure, both the MnN_6 and FeC_6 octahedra are strongly distorted: the MnN_6 octahedra is two-long/four-short type, while the FeC_6 octahedra is four-long/two-short type. This type of distortion is inconsistent with the infrared absorption spectra of the thermally quenched sample (Ref. 21), because the spectra suggest Mn^{2+}-Fe^{3+} valence state.
[23] The Debye-Scherrer powder rings are homogeneous even under pressure, and hence we can not ascribe the increase of intensity of the 202 reflection to preferred orientation.
[24] J.S. Langer, Ann. Phys. **41**, 108 (1967).
[25] Sh. Xu, Y. Moritomo, A. Machida, K. Ohoyama, K. Kato, and A. Nakamura, Phys. Rev. B **66**, 024420 (2002).
[26] P.W. Anderson and H. Hasegawa, Phys. Rev. **100**, 675 (1995).